Experimental Determination of Zonal Winds Driven by Tides

C. Morize,[1,2] M. Le Bars,[1] P. Le Gal,[1] and A. Tilgner[1,3]

[1]*Institut de Recherche sur les Phénomènes Hors Équilibre, UMR 6594, CNRS et Aix-Marseille Universités, 49 rue F. Joliot-Curie, Boîte Postale 146, 13384 Marseille Cedex 13, France*

[2]*Université Pierre et Marie Curie (Paris 6), Université Paris-Sud, CNRS. Laboratoire FAST, Bâtiment 502, Campus Univ., Orsay, F-91405, France*

[3]*Institute of Geophysics, University of Göttingen, Friedrich-Hund-Platz 1, 37077 Göttingen, Germany*

(Received 28 January 2010; revised manuscript received 22 April 2010; published 26 May 2010)

We describe a new phenomenon of zonal wind generation by tidal forcing. Following a recent theoretical and numerical analysis [A. Tilgner, Phys. Rev. Lett. **99**, 194501 (2007)], we present the first experimental evidence that the nonlinear self-interaction of a tidally forced inertial mode can drive an intense axisymmetric flow in a rotating deformed sphere. Systematic measurements of zonal flows are carried out by an embarked system of particle image velocimetry, allowing the determination of general scaling laws. These results are fully relevant for zonal winds generation in planets and stars, and illustrate a generic mechanism of geostrophic flow generation by periodic forcing.

DOI: 10.1103/PhysRevLett.104.214501 PACS numbers: 47.32.Ef, 05.45.−a, 96.15.Ef, 96.15.Wx

The fundamental role of gravitational tides in geo- and astrophysics has been the subject of multiple studies for several centuries. Beyond the well-known quasiperiodic flow of ocean water on our shores, tides are responsible for phenomena as varied as the synchronization of binary systems [1], the intense volcanism on Io, or the induction of a magnetic field by an elliptical instability [2,3]. We show here, for the first time experimentally, that tides could also participate in the generation of axisymmetric zonal winds in planetary cores and atmospheres, in addition to the already known mechanisms driven by convection [4] and stratified turbulence [5].

Rotating flows in planetary systems support oscillatory motions, called ''inertial waves'' [6]. These waves are the eigenmodes of rotating flows, but are usually damped by viscosity. Let us now consider the liquid core of a spinning planet and its orbiting moon (the same approach is valid for binary stars and for any planet-moon or star-planet system): deformations due to gravitational tides of azimuthal period $m = 2$, can potentially force an infinite number of $m = 2$ eigenmodes in the liquid core. Once a mode is forced, it is well known from precession studies [7] that the Ekman boundary layer which forms at the outer edge of the rotating fluid breaks down at critical latitudes where the group velocity of the excited inertial waves is tangent to the boundary. This Ekman layer breakdown is the source of conical oscillatory shear layers which penetrate the interior flow [8,9]. Besides, a geostrophic circulation is also excited [10], coming from the nonlinear self-interaction of the excited inertial mode. Greenspan [11] showed however that nonlinear interactions of inviscid inertial modes cannot produce any geostrophic flow. Viscosity modifies this classical picture and gives rise to intense axisymmetric cylindrical shear layers, parallel to the rotation axis [12–14]. Note that in the context of precessional flows, the amplitudes of the geostrophic flow measured by Malkus [10] or by Cardin and Olson [15] are 3 times larger than expected, attesting the real need of quantitative measurements of such geostrophic flows.

The same mechanism of zonal wind generation must exist for tidal forcing. Indeed, once a mode $m = 2$ is forced, its nonlinear self-interaction excites modes of azimuthal period $m = 4$ and $m = 0$, which can drive an intense axisymmetric flow. First considering that the tidal companion is fixed, which means that critical latitudes are exactly at the poles, Suess [16] revealed the existence of a polar counterrotating vortex, as well as a second axisymmetric shear layer at half the radius of the sphere, whose origin is still unknown. If now the tidal companion rotates at an independent orbital velocity, other inertial waves may be excited. A systematic scan of the orbital velocity allows the excitment of several inertial modes of frequency ω_{mode} when the orbital frequency $\Omega_{\mathrm{orbit}} = \omega_{\mathrm{mode}}/2$. The factor 2 comes from the fact that an $m = 2$ tidal deformation of period Ω_{orbit} excites a mode twice per complete rotation. This mechanism would then lead to the breakdown of the Ekman layer and the formation of geostrophic cylinders whose location depends on the ratio between the orbital and spin velocities. This was verified in a recent numerical analysis of Tilgner [17], by artificially injecting energy in the $m = 2$ inertial modes. The purpose of this letter is to validate this mechanism experimentally, taking into account a realistic tidal-like boundary deformation.

Our experimental setup that mimics a tidally deformed rotating fluid body is sketched in Fig. 1. It consists in a hollow deformable sphere, of radius $R = 10$ cm, which was molded in a transparent silicone gel. The sphere is filled with water and set in rotation about its vertical axis (Oz) with a constant angular velocity Ω_{spin} up to 150 rpm $\pm 0.3\%$. The spinning sphere is elliptically deformed by

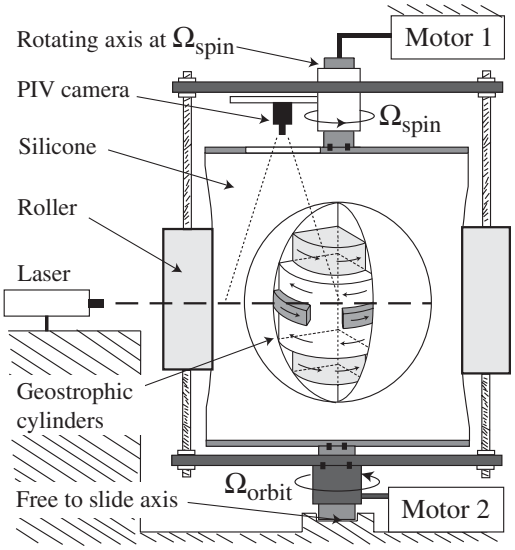

FIG. 1. Schematic of the experimental setup. The PIV camera is in the spin frame rotating with the deformed sphere; the two cylindrical rollers are in the orbital frame and the laser and the two motors are in the laboratory frame.

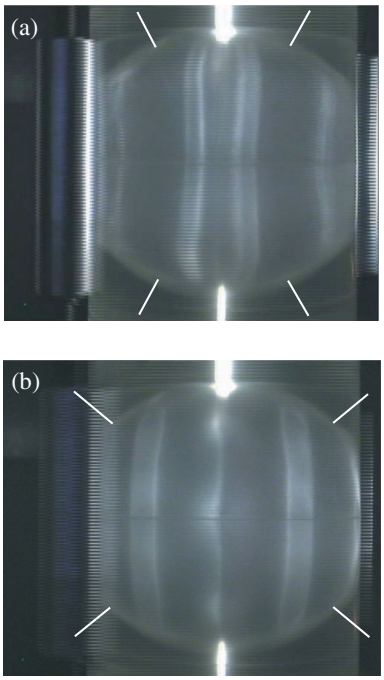

FIG. 2 (color online). Visualizations of intense axisymmetric flows using Kalliroscope flakes illuminated by a vertical meridional laser sheet. The observed bands correspond to the intersection of the excited geostrophic cylinders sketched in Fig. 1 with the visualization plane. The two photographs have been obtained for $E = 6 \times 10^{-5}$, $\epsilon = 0.04$ and for (a) $\Omega_R = 0.18$ and (b) $\Omega_R = 0.38$, corresponding to half the frequency of two $m = 2$ eigenmodes of the sphere. The white dots indicate the location of the theoretical critical latitudes.

two vertical cylindrical rollers. The tidal deformation is perpendicular to the rotation axis and is orbiting at an independent constant angular velocity Ω_{orbit} up to 100 rpm $\pm 0.3\%$. We use Ω_{spin}^{-1} as a timescale and R as a length scale. Such a system is then fully defined by three dimensionless numbers: the Ekman number $E = \nu/\Omega_{spin}R^2$, where ν is the kinematic fluid viscosity, the ratio of the orbital and spin angular velocities $\Omega_R = \Omega_{orbit}/\Omega_{spin}$, and the eccentricity of the ellipsoid ϵ. For the present experiment, the Ekman number has been varied in the range $[9 \times 10^{-4}; 3 \times 10^{-5}]$ while ϵ lies in the range [0.01; 0.08] with an accuracy of 3×10^{-3}.

Visualizations with anisotropic particles (Kalliroscope flakes) are made in a meridional plane. Particles are illuminated by a laser sheet, of thickness 3 mm, produced by a continuous laser (4 W) in a plane coinciding with the rotation axis. In the present work, we select the orbital velocity in the prograde direction in order to avoid the elliptical instability [18] and to isolate the mechanism of zonal wind driven by tides. But if an elliptical instability is present, we expect the same mechanism to superimpose on it. Visualizations with Kalliroscope flakes corresponding to two different modes are shown in Fig. 2. The illuminated parts of the fluid correspond to coherent orientation of flakes associated with a shear zone. There is no evidence of the conical structures of the internal flow. We expect this to be due to the lack of time for flakes to align in the oscillatory conical shear. Flakes only feel the stationary component of the flow, hence highlighting the geostrophic circulations. The shape, location and intensity of these shear cylinders depend on the excitation frequency. Note that as in the experiment of Suess [16], in addition to the expected shear layers, our flakes visualizations revealed additional, albeit much weaker, geostrophic cylinders, for instance at three-quarter of the radius of the deformed sphere in Fig. 2(a) and at the poles in Fig. 2(b). These additional shear layers may be due to harmonic waves of azimuthal period $m = 4$ and to a $m = 1$ forcing due to a slight dissymmetry of the experiment.

In addition to the purely qualitative flakes visualizations, measurements of velocity fields are obtained in the equatorial plane using a corotating particle image velocimetry (PIV) system. Water is seeded by Optimage particles of 100 μm in diameter and of density $1 \pm 2\%$. A miniature wireless CMOS camera (2 cm $\times$ 2 cm), of resolution 576×768 pixels, is installed on the rotating frame and measurements are made from above through the transparent top surface. The PIV data are acquired using a video transmitter-receptor system. Velocity fields are defined on a 45×60 grid in a semi equatorial section, with a spatial resolution of 3 mm close to the laser sheet thickness. Since the expected geostrophic circulations are time independent, velocity fields are time-averaged over 500 complete rotations of the deformed sphere, which eliminates the time dependent component of the flow and significantly enhances the signal-to-noise ratio. Figure 3 shows two velocity

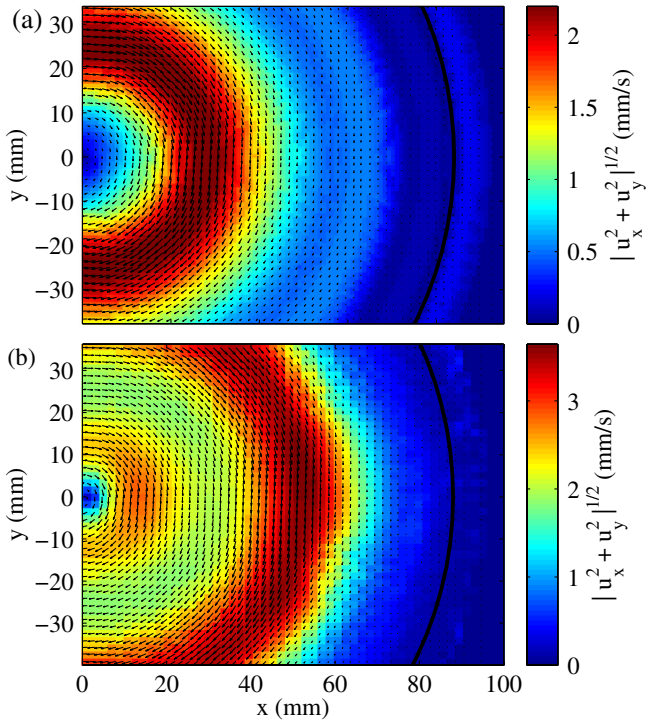

FIG. 3 (color online). Velocity fields obtained by PIV in equatorial plane for the same parameters as in Fig. 2. The background is colored as the norm of the horizontal velocity. Note that because of an undetectable area near the boundaries due to optical deformations related to the spherical silicone-water interface, the apparent boundary of the spheroid is located here at $r = 85$ mm.

fields obtained for the same parameters as in Fig. 2. Velocity fields exhibit axisymmetric flows which are mainly azimuthal. The system rotation is anticlockwise, so that zonal flows correspond here to anticyclonic circulations. An averaged azimuthal velocity profile, computed from Fig. 3(b) and its corresponding radial shear $\tau_{r,\phi} = \frac{\partial u_\phi}{\partial r} - \frac{u_\phi}{r}$ calculated in cylindrical coordinates, are plotted in Fig. 4 as a function of the radial distance, together with the location of the Kalliroscope band deduced from picture 2(b). We observe a very good agreement between PIV measurements and flakes visualizations. The vertical shear layers are centered on the local maxima of the radial shear and the illuminated parts of picture 2(b) correspond to flakes oriented in regions of positive gradient of the geostrophic velocity.

The maximal azimuthal velocity contained in geostrophic cylinders is plotted on Fig. 5 as a function of the normalized orbital frequency. The flow amplitude is negligible except when the orbital frequency resonates with an eigenmode of the sphere. The peak around $\Omega_R = 0$ corresponds to the spinover mode of the elliptical instability [18]. Its amplitude is huge in comparison to zonal winds and represents up to 20% of the angular velocity of the boundary in the present case. The five others energy peaks

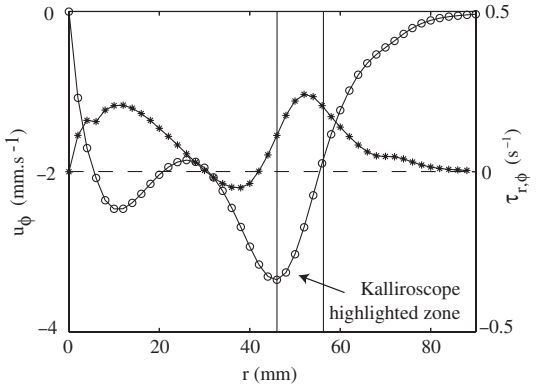

FIG. 4. Azimuthal velocity (o) and its corresponding radial shear $\tau_{r,\phi}$ (*) calculated from the velocity fields of Fig. 3(b). The area between the two vertical full lines corresponds to the thickness of the lateral vertical bands deduced from Fig. 2(b), taking into account the optical deformations.

correspond to the axisymmetric flows of interest here. The resonance peaks are very thin and are observed as expected for orbital frequencies in excellent agreement with half the frequencies of a full sphere $m = 2$ eigenmodes, indicated by vertical dashed lines. Velocity fields similar to those of Fig. 3 have been obtained for all the other resonances investigated in the course of this study. Note that we do not observe geostrophic circulations for modes with small length scale (i.e., with a degree of Legendre polynomial $l \geq 8$ in the notation of Greenspan [6]), as these modes are probably damped by viscous effects for the Ekman numbers reached in our setup.

Figure 6 shows the dependence of the maximal azimuthal velocity in zonal flows as a function of the eccentricity and the Ekman number. As predicted by Busse [7] for precession, the geostrophic velocity scales as the square of the amplitude of the boundary-layer flow, yielding in our case to a dependence with ϵ^2 as shown in Fig. 6(a). The Ekman number dependence of the geostrophic velocity can

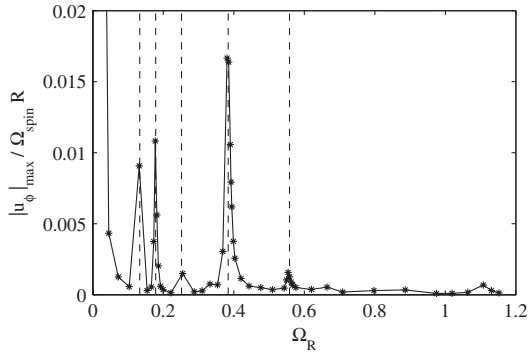

FIG. 5. Maximal azimuthal velocities of zonal flows normalized by the angular velocity of the ellipsoid as a function of the normalized orbital velocity for $E = 6 \times 10^{-5}$ and $\epsilon = 0.04$. Vertical dashed lines correspond to half the frequency of the $m = 2$ eigenmodes of the sphere.

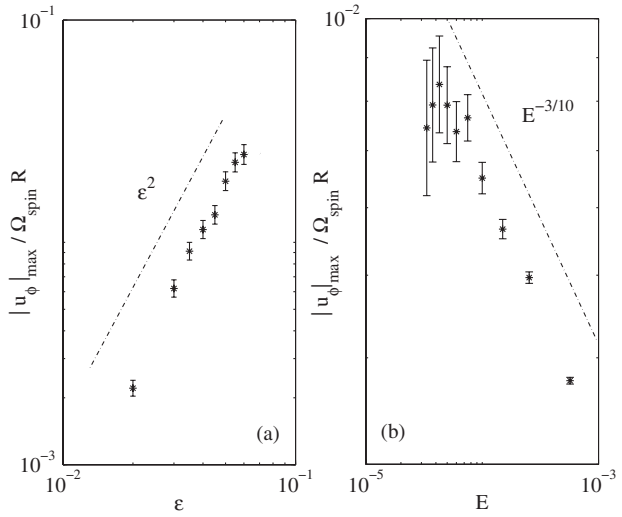

FIG. 6. Maximum azimuthal velocity contained in the geostrophic flow normalized by ($\Omega_{spin}R$) (a) as a function of the eccentricity for $E = 6 \times 10^{-5}$ and $\Omega_R = 0.38$, and (b) as a function of the Ekman number for $\epsilon = 0.04$ and $\Omega_R = 0.38$. Dashed-dotted lines correspond to theoretical scalings, and error bars are equal to the rms value of the measures which ranges between 5%–15%.

also be determined following precession studies [13], by balancing the viscous damping of the geostrophic cylinder in the boundary layer of thickness $O(E^{1/2})$, with the dominant nonlinear term $u_r \partial u_\phi / \partial r$ integrated in the Ekman layer of thickness $O(E^{2/5})$ around critical latitudes. It follows that the geostrophic velocity scales as $E^{-3/10}$. As can be seen on Fig. 6(b), the variation of the azimuthal velocity is compatible with this $E^{-3/10}$ power law. Note that a stronger dependence on E is expected in the presence of a core [17] because in a spherical shell, the eigenmodes become singular [19] in the limit of vanishing E, which consequently increases their nonlinear self-interaction. This will be the subject of a future experimental study.

In summary, this work presents the first experimental evidence that the nonlinear self-interaction of a tidally forced inertial mode can drive intense axisymmetric flows. Our measurements of zonal winds generated by tides have been carried out using an embarked PIV system. The geostrophic velocity is found to vary as $\epsilon^2 E^{-3/10}$. The mechanism revealed here for a tidal deformation of the rigid external boundary of our rotating fluid sphere is fully generic. In fact, each resonant periodic forcing (e.g., additional tides, precession, nutation, etc.) on any external or internal interface possessing an Ekman layer, will generate its own geostrophic shear cylinder. The resulting flow will then correspond to the superimposition of all the contributions, as illustrated for instance in Fig. 7, where an ecliptic inclination has been added. Such a mechanism could therefore take place almost generically in the liquid cores of

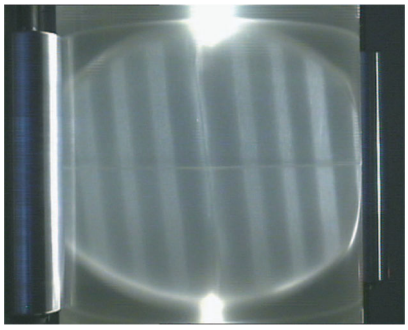

FIG. 7 (color online). Kalliroscope visualization of a resonant tidal forcing at $E = 10^{-5}$ for a spin axis inclined by an angle $\sim 5^\circ$ compared to the axis of the deformation. This corresponds in astrophysical terms to an inclination of the ecliptic plane. Forcing with azimuthal period $m = 2$ and $m = 1$, as well as possible harmonics $m = 3$, $m = 4$, etc., leads to the apparition of numerous shear cylinders.

planets, but also in the atmospheres of gas giants such as Jupiter, where it would constitute an additional source of zonal winds generation in complement to the already suggested competing models [4,5]. More generally, our results obtained here in the case of tidal forcing involve subtle and fundamental fluid flow mechanisms linked to nonlinearities that are fully relevant to any harmonic forcing of any flow.

We acknowledge J. Noir for fruitful discussions. This work was supported by the program SEDIT of INSU and by the ANR IMAGINE-07-BLAN-0182.

[1] M. Le Bars *et al.*, PEPI **178**, 48 (2010).
[2] R. R. Kerswell and W. V. R. Malkus, Geophys. Res. Lett. **25**, 603 (1998).
[3] W. Herreman *et al.*, Phys. Fluids **21**, 046602 (2009).
[4] F. H. Busse, Icarus **29**, 255 (1976).
[5] G. P. Williams, J. Atmos. Sci. **36**, 932 (1979).
[6] H. Greenspan, *The Theory of Rotating Fluids* (Cambridge University Press, Cambridge, England, 1968).
[7] F. H. Busse, J. Fluid Mech. **33**, 739 (1968).
[8] R. R. Kerswell, J. Fluid Mech. **298**, 311 (1995).
[9] J. Noir *et al.*, Geophys. Res. Lett. **28**, 3785 (2001).
[10] W. V. R. Malkus, Science **160**, 259 (1968).
[11] H. Greenspan, J. Fluid Mech. **36**, 257 (1969).
[12] J. Vanyo *et al.*, Geophys. J. Int. **121**, 136 (1995).
[13] J. Noir *et al.*, J. Fluid Mech. **437**, 283 (2001).
[14] S. Lorenzani and A. Tilgner, J. Fluid Mech. **447**, 111 (2001).
[15] P. Cardin and P. Olson, *Treatise of Geophysics* (Elsevier, New York, 2007), Vol. 8, Chap. 11, p. 319.
[16] S. T. Suess, J. Fluid Mech. **45**, 189 (1971).
[17] A. Tilgner, Phys. Rev. Lett. **99**, 194501 (2007).
[18] M. Le Bars *et al.*, J. Fluid Mech. **585**, 323 (2007).
[19] M. Rieutord *et al.*, Phys. Rev. Lett. **85**, 4277 (2000).